Enhanced dissolution of nitrogen during gas tungsten arc welding of steels

T. A. Palmer and T. DebRoy

Although nitrogen concentrations at levels much higher than Sieverts' Law predictions during the arc welding of iron and steel are well established, there is currently no commonly accepted methodology to determine this concentration quantitatively. The nature and concentrations of various species in the plasma phase above the weld pool surface are therefore investigated in the present work using both theoretical and experimental techniques. A comprehensive thermodynamic analysis of the nitrogen containing plasma phase of a gas tungsten welding arc shows that ionised species dominate close to the electrode, whereas neutral monatomic and diatomic nitrogen are the primary species near the metal surface at plasma temperatures as low as 5000 K. When oxygen is added to a nitrogen containing plasma, the resulting nitrogen concentration in the weld metal is further enhanced. Definitive proof is provided for a mechanism in which nitrogen and oxygen species interact in the plasma phase at temperatures below 6000 K, resulting in a significant increase in the concentration of monatomic nitrogen. Furthermore, at plasma temperatures as low as 5000 K, the equilibrium monatomic nitrogen partial pressure is sufficiently high to cause nitrogen saturation in the weld metal. Emission spectroscopy of glow discharge plasmas validates both the species density calculations and the presence of NO in the nitrogen and oxygen containing plasmas.

The authors are in the Department of Materials Science and Engineering, Penn State University, University Park, PA 16802, USA. *Manuscript received 17 November 1997; in final form 15 December 1997.*

INTRODUCTION

Nitrogen solubility in excess of Sieverts' Law is observed when a nitrogen containing plasma comes into contact with a metal. Experimental studies of nitrogen dissolution into the weldment and the effect of changes in welding parameters or alloy composition on the final nitrogen concentration have been performed over the past several decades.[1,32] Gedeon and Eagar[33] and other researchers[28,34,35] have explained the enhanced concentration of hydrogen and other diatomic gases in the weld metal by assuming the dominant role of monatomic gaseous species in the plasma phase. If the concentration of the monatomic species in the gas phase near the weld pool is known, the species concentration can then be estimated by considering the equilibrium between the monatomic gas and metal.

Dissociation of diatomic nitrogen into monatomic nitrogen species in the welding arc has been well established.[31,36] The resulting concentration of atomic nitrogen in the plasma is higher than would be obtained solely from consideration of thermal equilibrium between these two species at the temperature and pressure prevailing at the metal surface. Rather, the amount of monatomic nitrogen in the plasma phase depends on the nature of the power source, the energy dissipated, the overall system geometry, and the nature of the diatomic gas.[34] It is very difficult to quantify many of these factors which determine the species concentrations in the welding arc, resulting in many problems in calculating the residual nitrogen concentration in the weld metal.

Taking these difficulties into account, Gedeon and Eagar[33] have developed a model which considers both the dissociation and absorption reactions. The dissociation of the diatomic gas is governed by the temperature of the plasma phase adjacent to the weld pool surface, whereas the absorption reaction is governed by the surface temperature of the weld pool. Based on this model, several available plasma metal systems have been analysed, and the enhanced nitrogen solubility in the weld metal is explained by a superequilibrium concentration of monatomic species above the weld metal.[34]

Uda and Wada[12] also recognised the complexity of the interaction between the plasma phase and the weld metal. They divided the absorption reaction into three areas: the bulk plasma area, a boundary layer adjacent to the weld metal, and the weld metal itself. Within the boundary layer, the temperature is considered to be nearly equal to the melting point of the molten metal. The experimentally observed nitrogen concentrations under arc melting conditions correspond to a partial pressure of atomic nitrogen obtained by equilibrium thermal dissociation of diatomic nitrogen at about 3000 K. This temperature is much lower than the temperatures in the arc column.

It has long been well known that the presence of a small amount of oxygen enhances the nitrogen concentration in the weld metal.[1,2,17,25,37,38] This behaviour is illustrated in Fig. 1. Some authors[25,37] have hypothesised that the presence of NO in these plasmas, resulting from the interaction between nitrogen and oxygen, is the main contributor to this enhancement. Currently there is no unified theory to explain this behaviour. Furthermore, there is no experimental evidence available for the presence of NO. Detailed calculation of species concentrations in an $Ar-N_2-O_2$ system, considering possible reaction between the nitrogen and oxygen, can provide a definitive understanding of this behaviour.

A number of researchers have investigated the characteristics of the plasma phase in the arc column.[15,25,38,40,44] Theoretical studies of the number densities of various species in a plasma phase include those performed by Dunn and Eagar,[42] who investigated inert gaseous plasmas, and by Drellishak and co-workers,[43,44] who investigated both inert gaseous and pure nitrogen and oxygen plasmas at atmospheric pressures. Dunn and co-workers[41,42] calculated the electron densities and the resulting transport properties of argon and helium plasmas with small additions of metal vapours. To calculate these transport properties, only ionisation reactions require consideration, given the dominant role of the electron density in determining the electrical and

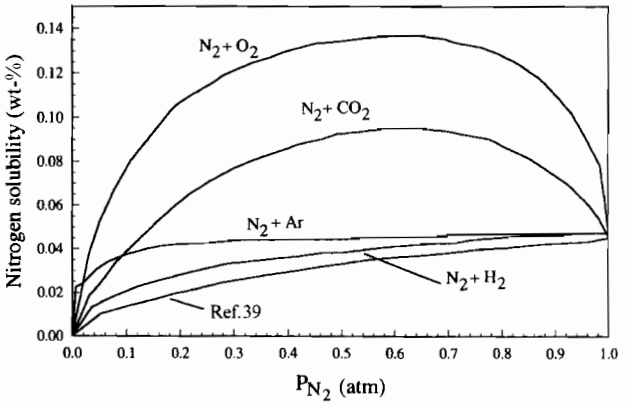

1 Role of oxygen and oxygen containing species in further enhancement of nitrogen concentration in weld pool: after Ref. 2

thermal conductivities. They therefore calculated species and electron densities in the plasma phase using the Saha–Eggert relationship and the ideal gas law. Fast[36] investigated the dissociation of nitrogen in the welding arc based on thermodynamic calculations and ignoring the role of ionisation reactions. The calculation of the number densities for both nitrogen molecules and atoms over a range of temperatures was carried out based on fundamental spectroscopic data. These studies provided a database for the distribution of species in a plasma over a range of temperatures but have not been extended to temperatures approaching those on the weld pool surface. A rigorous quantitative analysis of the plasma phase to determine the concentration of various nitrogen bearing species has not been performed.

The number densities of various gaseous species calculated in the present work have been used to understand nitrogen dissolution in the weld pool. To provide a complete picture of the species present in the welding arc plasma, both dissociation and ionisation reactions have been considered. The species densities for nitrogen, oxygen, argon, and helium plasmas have been calculated for both pure gases and mixtures. In addition, the role of oxygen in the enhanced nitrogen dissolution reaction is also investigated using these calculations. Finally, the nitrogen absorption reaction during arc welding is examined by considering the interaction between the plasma phase and the weld pool surface during gas tungsten arc (GTA) welding. Experimental verification of these calculations is achieved through the use of emission spectroscopic analysis of glow discharge plasmas.

CALCULATION METHODOLOGY

To calculate the number densities of species present in the plasma phase, ionisation and dissociation reactions for both diatomic and monatomic species must be considered simultaneously. Furthermore, the balance of charge throughout the system and the conservation of mass must be considered. The ionisation reactions of interest for a pure nitrogen plasma are as follows

$$N_2 = N_2^+ + e^- \quad \ldots \quad (1)$$

$$N = N^+ + e^- \quad \ldots \quad (2)$$

Assuming local thermodynamic equilibrium, the relation between the various species densities can be expressed from the Saha–Eggert relation[42–44] as follows

$$\frac{n_e n_{N_2^+}}{n_{N_2}} = \frac{2(2\pi m_e kT)^{3/2}}{h^3}\frac{Z_{N_2^+}}{Z_{N_2}}\exp(-\varepsilon_{N_2}/kT) \quad \ldots \quad (3)$$

$$\frac{n_e n_{N^+}}{n_N} = \frac{2(2\pi m_e kT)^{3/2}}{h^3}\frac{Z_{N^+}}{Z_N}\exp(-\varepsilon_N/kT) \quad \ldots \quad (4)$$

where n_e is the electron density and n_{N_2}, $n_{N_2^+}$, n_N, and n_{N^+} are the number densities for each of the respective nitrogen species, m_e is the rest mass of an electron, k is the Boltzmann constant, T is the electron temperature, h is Planck's constant, Z_{N_2}, $Z_{N_2^+}$, Z_N, and Z_{N^+} are the partition functions for the respective nitrogen species, and ε_{N_2} and ε_N are the ground state energies for the nitrogen molecule and atom, respectively. The partition functions[36,42,43] for a number of pure species are calculated in Appendix 1.

The dissociation reaction of diatomic nitrogen and its equilibrium constant K are presented in equations (5) and (6), respectively

$$N_2(g) \rightarrow 2N(g) \quad \ldots \quad (5)$$

$$K_6 = \frac{p_N^2}{p_{N_2}} = \frac{n_N^2}{n_{N_2}}\left(\frac{RT}{N_A}\right) \quad \ldots \quad (6)$$

where p_N is the partial pressure of monatomic nitrogen, p_{N_2} is the partial pressure of diatomic nitrogen, R is the gas constant, and N_A is Avogadro's number. At temperatures commonly used for conventional materials processing, the free energy values are available and the value of K_6 can be readily calculated. In contrast, accurate thermodynamic data are not readily available for the high temperatures commonly found in the welding plasma. A recourse is to calculate the necessary data and the procedure used is presented in Appendix 2.

In pure nitrogen plasma, there are five species concentrations, i.e. n_{N_2}, $n_{N_2^+}$, n_N, n_{N^+}, and n_e, to be determined. Thus, in addition to equations (3), (4), and (6), two more equations must be developed, one based on the principle of quasineutrality in the plasma phase and the other based on the conservation of mass

$$n_e = n_{N_2^+} + n_{N^+} \quad \ldots \quad (7)$$

$$N_A\left(\frac{P}{RT}\right) = n_{N_2} + 2n_{N_2^+} + n_N + 2n_{N^+} \quad \ldots \quad (8)$$

where P is the total pressure. Since the total number of species present in the plasma phase is based on the ideal gas law, a decrease in the number density of particles with an increase in temperature should be expected. Equations (3), (4), and (6)–(8) can be solved simultaneously to obtain values of n_{N_2}, $n_{N_2^+}$, n_N, n_{N^+}, and n_e. To obtain the species densities over the range of temperatures commonly found in the welding arc, the system of equations must be solved simultaneously for each individual temperature.

When the plasma contains other gases, such as oxygen, additional species densities must be considered. Table 1 gives the species of interest for each of the pure gases analysed. For pure oxygen, the species densities to be determined include n_{O_2}, $n_{O_2^+}$, n_O, n_{O^+}, $n_{O^{++}}$, and n_e. These are obtained from the solution of the following system of six equations

$$\frac{n_e n_{O_2^+}}{n_{O_2}} = \frac{2(2\pi m_e kT)^{3/2}}{h^3}\frac{Z_{O_2^+}}{Z_{O_2}}\exp(-\varepsilon_{O_2}/kT) \quad (9)$$

$$\frac{n_e n_{O^+}}{n_O} = \frac{2(2\pi m_e kT)^{3/2}}{h^3}\frac{Z_{O^+}}{Z_O}\exp(-\varepsilon_O/kT) \quad (10)$$

Table 1 Summary of species considered in species density calculations for oxygen, nitrogen, argon, and helium

Input gas	Species considered
Argon	Ar, Ar^+, Ar^{2+}
Helium	He, He^+
Nitrogen	N_2, N_2^+, N, N^+
Oxygen	O_2, O_2^+, O, O^+, O^{++}

$$\frac{n_e n_{O^{++}}}{n_{O^+}} = \frac{2(2\pi m_e kT)^{3/2}}{h^3}\frac{Z_{O^{++}}}{Z_{O^+}}\exp(-\varepsilon_{O^+}/kT) \quad (11)$$

$$K_{12} = \frac{p_O^2}{p_{O_2}} = \frac{n_O^2}{n_{O_2}}\left(\frac{RT}{N_A}\right) \quad (12)$$

$$n_e = n_{O_2^+} + n_{O^+} + n_{O^{++}} \quad (13)$$

$$N_A\left(\frac{P}{RT}\right) = n_{O_2} + 2n_{O_2^+} + n_O + 2n_{O^+} + 3n_{O^{++}} \quad (14)$$

For pure monatomic inert gases such as argon and helium it is not necessary to consider any dissociation reaction. The argon species densities, i.e. n_{Ar}, n_{Ar^+}, $n_{Ar^{++}}$, and n_e, can be determined by the solution of the following system of equations

$$\frac{n_e n_{Ar^+}}{n_{Ar}} = \frac{2(2\pi m_e kT)^{3/2}}{h^3}\frac{Z_{Ar^+}}{Z_{Ar}}\exp(-\varepsilon_{Ar}/kT) \quad (15)$$

$$\frac{n_e n_{Ar^{++}}}{n_{Ar^+}} = \frac{2(2\pi m_e kT)^{3/2}}{h^3}\frac{Z_{Ar^{++}}}{Z_{Ar^+}}\exp(-\varepsilon_{Ar^+}/kT) \quad (16)$$

$$n_e = n_{Ar^+} + 2n_{Ar^{++}} \quad (17)$$

$$N_A\left(\frac{P}{RT}\right) = n_{Ar} + 2n_{Ar^+} + 3n_{Ar^{++}} \quad (18)$$

This same methodology is used to calculate the species densities for helium, but only three species densities require calculation, i.e. n_{He}, n_{He^+}, and n_e, since only a single ionisation level needs to be considered. The following three equations are thus solved to determine the number densities of these species

$$\frac{n_e n_{He^+}}{n_{He}} = \frac{2(2\pi m_e kT)^{3/2}}{h^3}\frac{Z_{He^+}}{Z_{He}}\exp(-\varepsilon_{He}/kT) \quad (19)$$

$$n_e = n_{He^+} \quad (20)$$

$$N_A\left(\frac{P}{RT}\right) = n_{He} + 2n_{He^+} \quad (21)$$

When considering binary, ternary, or higher order gas mixtures, the particle densities of the individual species can be calculated by considering a system of equations involving both the ionisation and dissociation reactions and the overall charge and mass balances. For example, the species densities of an Ar–N_2–O_2 gas mixture at 1 atm total pressure can be determined by solving a system of equations which takes into account the reactions for argon (equations (15) and (16)), nitrogen (equations (3), (4), and (6)), oxygen (equations (9)–(12)), and the overall charge and mass balances in equations (22)–(25).

$$n_e = X_{Ar}(n_{Ar^+} + 2n_{Ar^{++}}) + X_{N_2}(n_{N_2^+} + n_{N^+}) + X_{O_2}(n_{O_2^+} + n_{O^+} + 2n_{O^{++}}) \quad (22)$$

$$X_{Ar}\left[N_A\left(\frac{P}{RT}\right)\right] = n_{Ar} + 2n_{Ar^+} + 3n_{Ar^{++}} \quad (23)$$

$$X_{N_2}\left[N_A\left(\frac{P}{RT}\right)\right] = n_{N_2} + n_{N_2^+} + n_N + n_{N^+} \quad (24)$$

$$X_{O_2}\left[N_A\left(\frac{P}{RT}\right)\right] = n_{O_2} + 2n_{O_2^+} + n_O + 2n_{O^+} + 3n_{O^{++}} \quad (25)$$

where X_{Ar}, X_{N_2}, and X_{O_2} are the mole fractions of argon, nitrogen, and oxygen, respectively in the feed gas into the welding arc.[42] Both pure gases and binary and ternary gas mixtures have been analysed using this methodology at total pressures of 1 atm and a broad temperature range indicative of the temperatures in the welding arc.

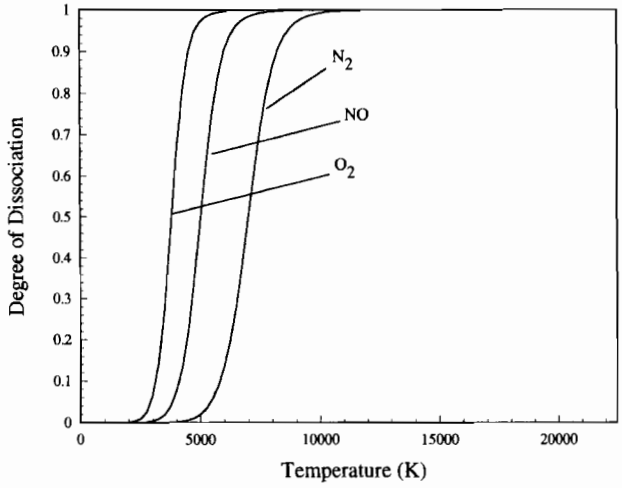

2 Comparison of computed values for extent of dissociation between N_2, O_2, and NO as function of temperature: value of 0 for degree of dissociation describes no dissociation occurring, and value of 1 describes complete dissociation

The above calculation scheme does not take into account the formation of any intermediate species, such as NO, in the plasma phase. Some authors[25,38] have hypothesised the presence of NO in plasmas containing nitrogen and oxygen, and several others[2,25,37,38] have reported a further increase in the nitrogen solubility in the weld metal with oxygen present in the plasma phase, for which the presence of NO is considered responsible. Once the NO species is formed in the plasma phase, it also undergoes dissociation and ionisation reactions, as shown in equations (26) and (28) below. When compared with the extent of dissociation of pure N_2 and O_2, NO is intermediate between the two (*see* Fig. 2)

$$NO \rightarrow N + O \quad (26)$$

$$K_{27} = \frac{p_N p_O}{p_{NO}} = \frac{n_N n_O}{n_{NO}}\left(\frac{RT}{N_A}\right) \quad (27)$$

$$NO \rightarrow NO^+ + e^- \quad (28)$$

$$\frac{n_e n_{NO^+}}{n_{NO}} = \frac{2(2\pi m_e kT)^{3/2}}{h^3}\frac{Z_{NO^+}}{Z_{NO}}\exp(-\varepsilon_{NO}/kT) \quad (29)$$

To calculate the various species densities resulting from considering the interaction between nitrogen and oxygen, all of the reactions for the dissociation and ionisation of nitrogen, oxygen, and NO must be solved along with the ionisation reactions for either argon or helium. For an Ar–$8N_2$–$2O_2$ system, the individual species densities can be determined by solving a system of equations which takes into account reactions for argon (equations (15) and (16)), nitrogen (equations (3), (4), and (6)), oxygen (equations (9)–(12)), NO (equations (27) and (29)), and the overall charge balance in equation (30) and mass balances in equations (23), (31), and (32).

$$n_e = X_{Ar}(n_{Ar^+} + 2n_{Ar^{++}}) + X_{N_2}(n_{N_2^+} + n_{N^+} + n_{NO^+}) + X_{O_2}(n_{O_2^+} + n_{O^+} + 2n_{O^{++}}) \quad (30)$$

$$X_{N_2}\left[N_A\left(\frac{P}{RT}\right)\right] = n_{N_2} + 2n_{N_2^+} + n_N + 2n_{N^+} + n_{NO} + 2n_{NO^+} \quad (31)$$

$$X_{O_2}\left[N_A\left(\frac{P}{RT}\right)\right] = n_{O_2} + 2n_{O_2^+} + n_O + 2n_{O^+} + 3n_{O^{++}} + n_{NO} + 2n_{NO^+} \quad (32)$$

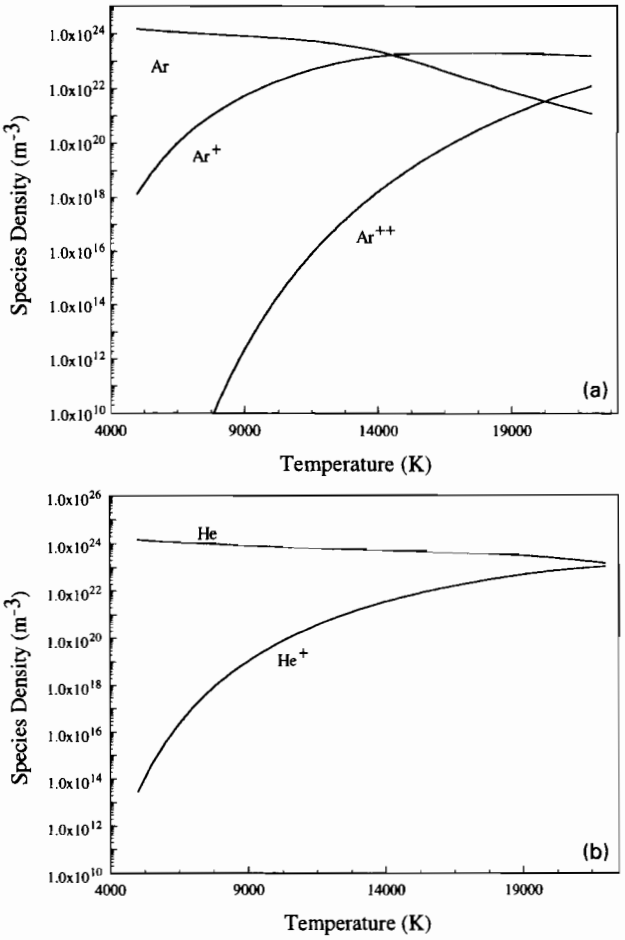

3 Computed species density for inert gases *a* argon and *b* helium as function of temperature

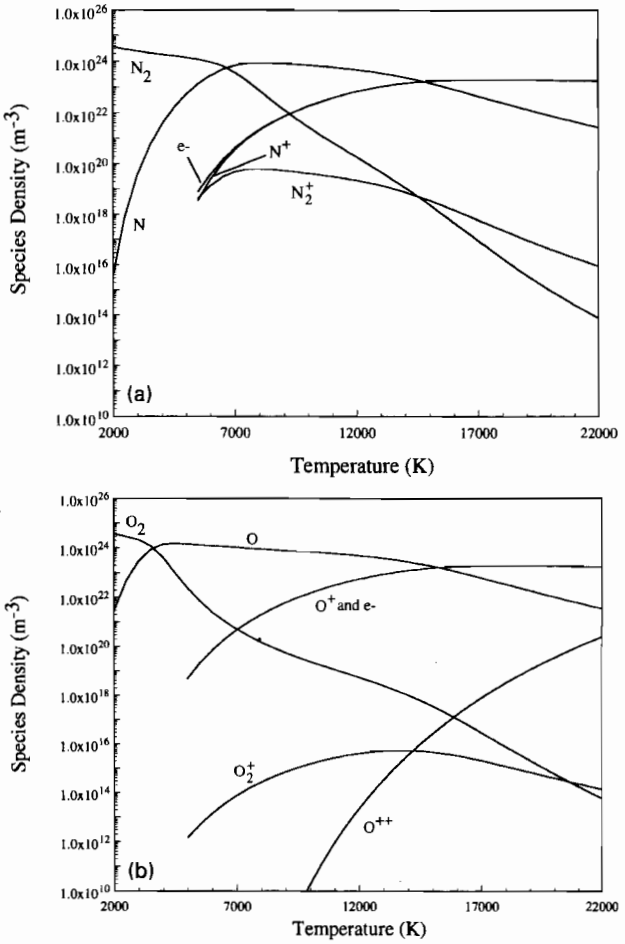

4 Computed species densities for *a* nitrogen and *b* oxygen species at 1 atm total pressure as function of temperature

RESULTS AND DISCUSSION

Before analysing gas mixtures, the calculation methodology was tested by comparing number densities for pure gases with those available in the literature. Figure 3*a* and *b* shows the species density distributions for argon and helium, respectively, in the temperature range from 4000 to 22 000 K. Since helium is much more difficult to ionise than argon, only the first ionisation level of helium, He^+, is considered, whereas both Ar^+ and Ar^{++} are considered for argon. Differences in the ionisation behaviour between argon and helium are consistent with their different ionisation potentials. Very little ionisation occurs at temperatures below 8000 K for argon and 14 000 K for helium. At higher temperatures, the concentration of the singly charged species increases. In pure argon plasmas, the singly charged argon ions dominate above 14 000 K. In contrast, the number density of the helium ions does not exceed that of the helium atoms for temperatures below 22 000 K. These results agree well with reported values. Thus, the calculation scheme provides accurate predictions.

Computed number densities of various nitrogen species are shown in Fig. 4*a* over a temperature range from approximately 2000 to 22 000 K. At temperatures below 6000 K, the extent of dissociation and ionisation is low and diatomic nitrogen dominates. In this temperature range, ionised species play no role and are not considered. Above approximately 7000 K, monatomic nitrogen is the dominant species, and N^+ dominates as the temperature is increased above 14 000 K. Oxygen, in contrast, dissociates and ionises much more readily than nitrogen, as shown in Fig. 4*b*. In this figure, monatomic oxygen dominates at temperatures much below 5000 K, whereas O^+ dominates at temperatures greater than approximately 14 000 K. Minor differences in the present calculated results and those available in the literature[42] can be attributed to the consideration of additional energy states for the ionised species and a more rigorous calculation scheme adopted in the present work, both of which lead to higher accuracy.

Temperatures in the arc column can vary depending on the welding conditions.[45–52] Several examples are shown in Fig. 5*a–d*, with the respective experimental conditions summarised in Table 2. High temperatures are observed close to the electrode and decrease as the workpiece is approached in all cases. For the temperature distributions shown in

Table 2 Summary of welding conditions leading to temperature distributions analysed for species distribution calculations

Fig.	Arc current, A	Arc voltage, V	Arc length, mm	Shielding gas	Electrode diameter, mm	Ref.
5*a*	150	Varied	2·0	Ar	2·38	45
5*b*	100	16	8	Ar	1·5	46
5*c*	100	Varied	5	Ar	3·2	49
5*d*	200	Varied	5	Ar	3·2	49

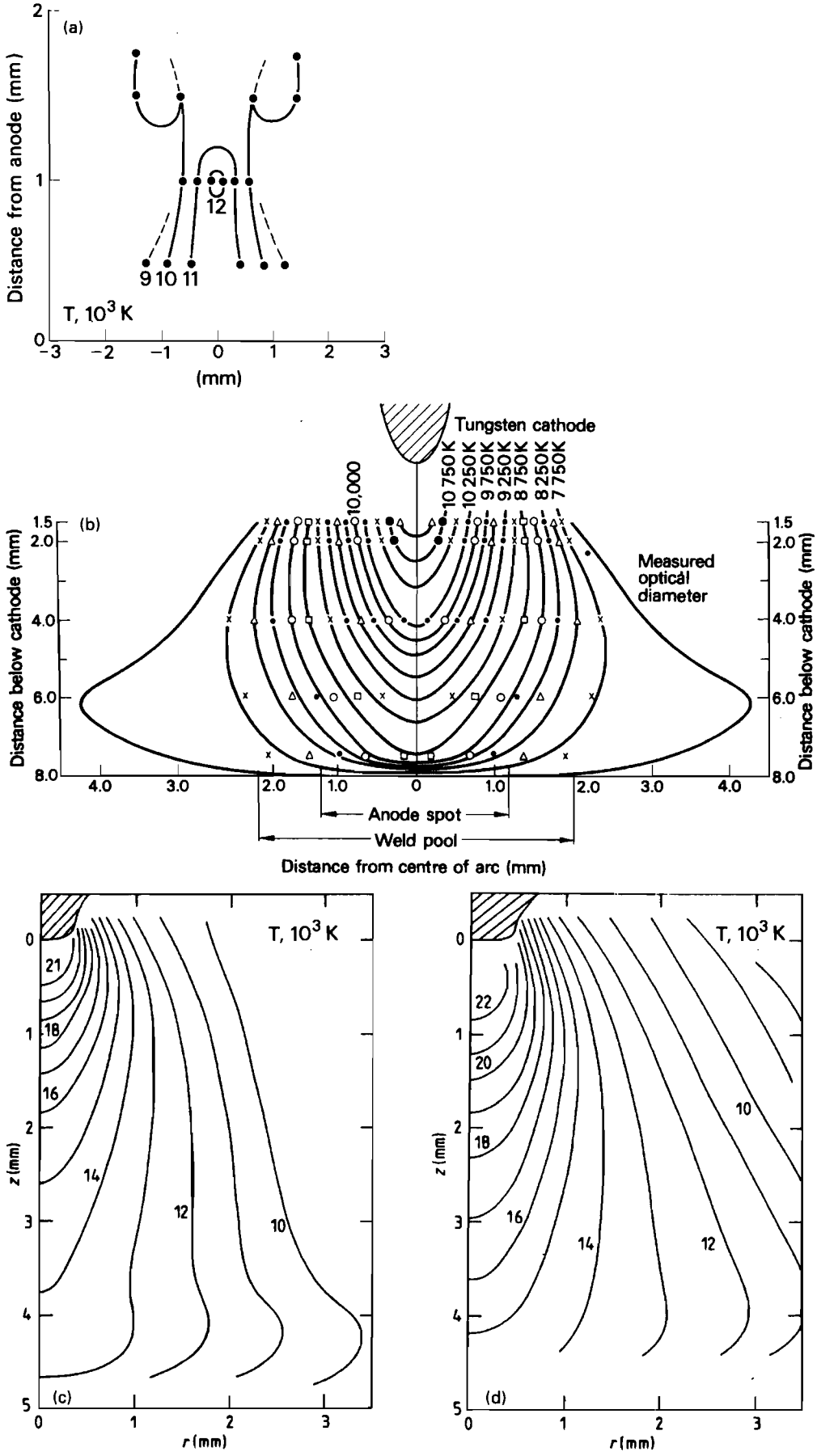

5 ***a*** **schematic diagram of spectroscopically measured temperatures in 100%Ar arc, with arc current of 150 A, and 30° vertex angle for electrode tip (after Ref. 45);** ***b*** **temperature distribution in arc column under gas tungsten arc (GTA) welding conditions for arc current of 100 A – temperatures in arc column were calculated using electrostatic probes (after Ref. 46);** ***c*** **temperature profile for 100 A argon arc (after Ref. 49);** ***d*** **temperature profile for 200 A argon arc (after Ref. 49)**

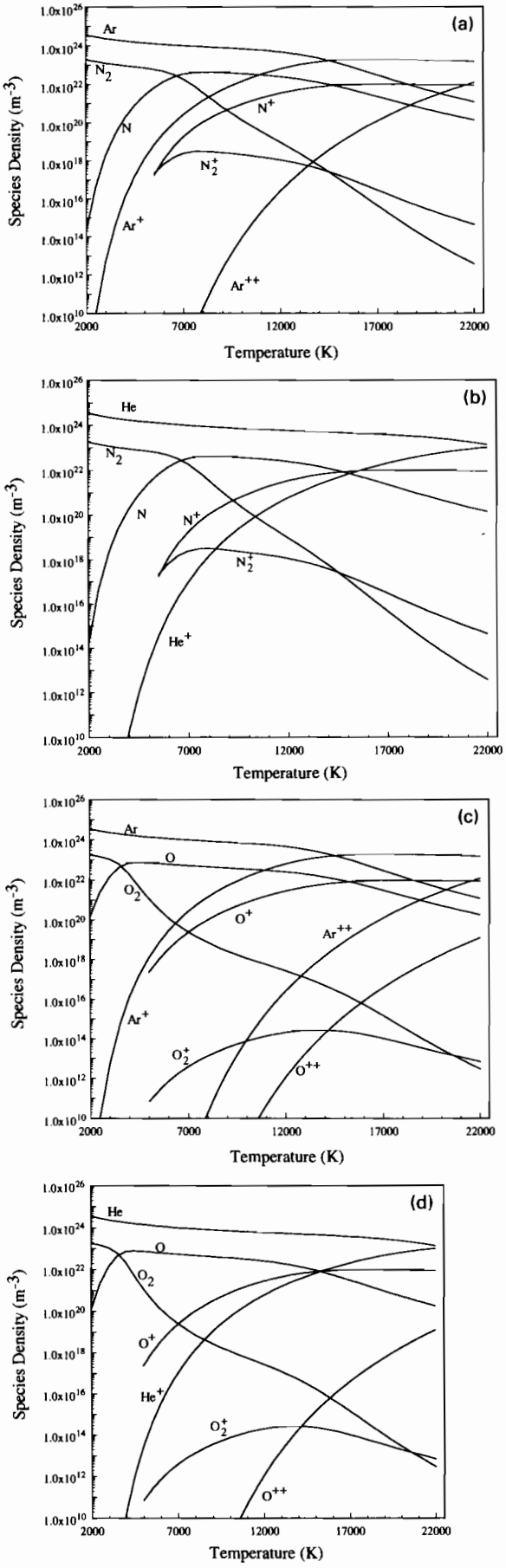

a Ar–$5N_2$; *b* He–$5N_2$; *c* Ar–$5O_2$; *d* He–$5O_2$

6 Computed species densities for two component systems as function of temperature

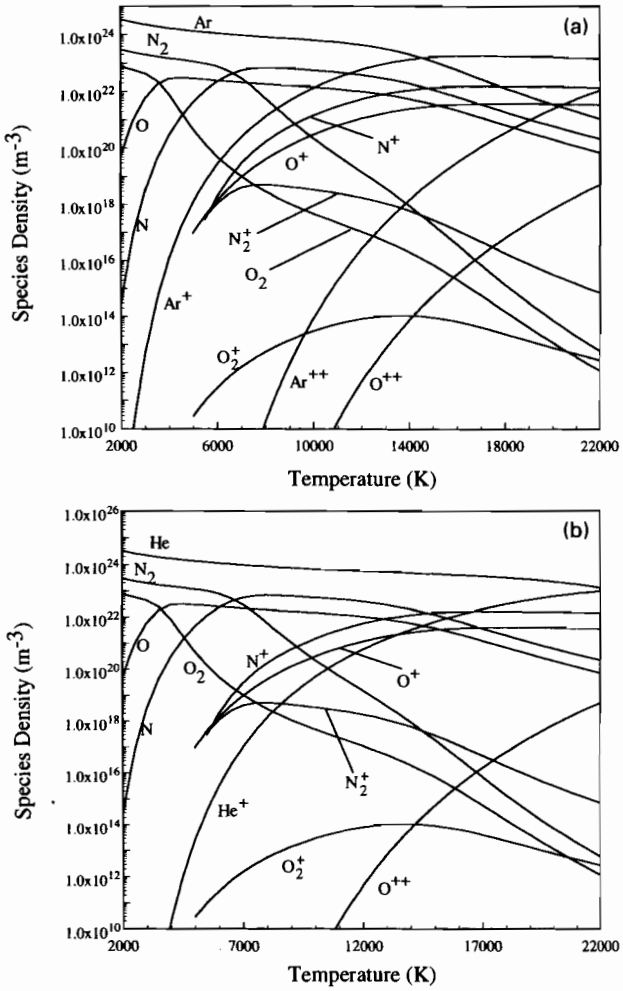

7 Computed species densities for three component systems consisting of *a* Ar–$8N_2$–$2O_2$ and *b* He–$8N_2$–$2O_2$, as function of temperature assuming no interaction

Fig. 5*a* and *b*, monatomic nitrogen (N) dominates throughout the arc column. Although the two temperature distributions are different, the temperatures are sufficiently high for significant dissociation of the diatomic nitrogen. In Fig. 5*c* and *d*, the temperatures at locations much closer to the electrode are of the order of 21 000 K and ionic nitrogen (N^+) dominates. Throughout the remainder of the plasma phase in the arc column, the temperatures are sufficiently high for significant dissociation of the diatomic nitrogen to occur and for monatomic nitrogen (N) to dominate. Therefore, ionised species tend to dominate at locations closer to the electrode, and neutral species are dominant as the workpiece is approached.

Atmospheric pressure nitrogen and oxygen arcs are not normally observed in welding applications; on the contrary, only small amounts of these gases are added, whether deliberately or not, to the welding arc. Therefore, calculations have been performed for inert gas plasmas with the addition of diatomic gases. Figure 6*a* and *b* show the species distributions for Ar–N_2 and He–N_2 mixtures. In each case, argon and helium species dominate across the range of temperatures considered. The choice of shielding gas affects the extent of ionisation at high temperatures. Similar calculated results for Ar–O_2 and He–O_2 mixtures are presented in Fig. 6*c* and *d*, and the same behaviour as that seen in Fig. 6*a* and *b* is observed.

Of even greater concern in practical welding operations is the addition of small amounts of air to the shielding gas during GTA welding. Since air is primarily composed of

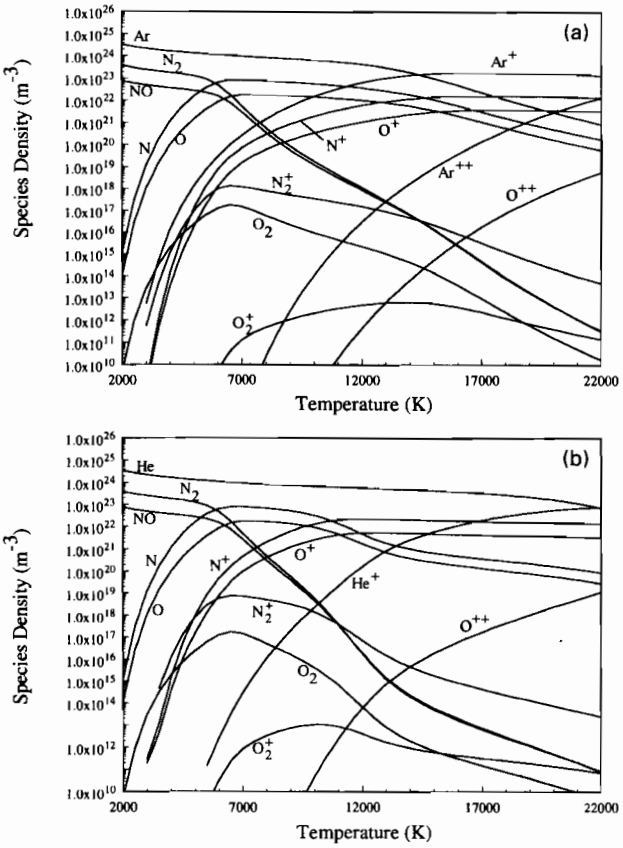

8 Computed species densities for three component systems consisting of *a* Ar–8N_2–2O_2 and *b* He–8N_2–2O_2, as function of temperature with interaction between nitrogen and oxygen

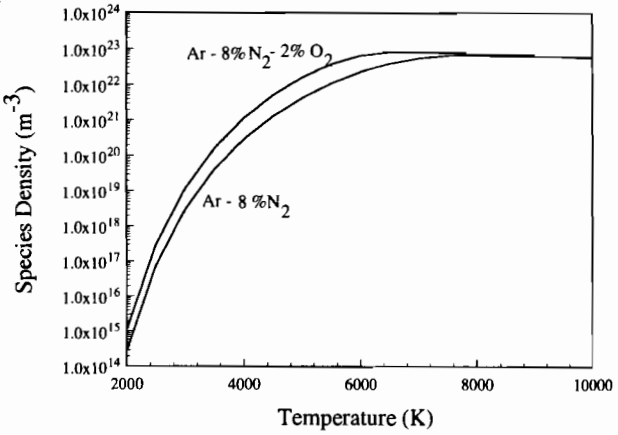

9 Comparison of computed number density of monatomic nitrogen for Ar–8N_2 and Ar–8N_2–2O_2 plasmas at electron temperatures below 8000 K

nitrogen and oxygen, Fig. 7*a* and *b* display the species density distributions for Ar–N_2–O_2 and He–N_2–O_2 mixtures, respectively, in which no interaction between the nitrogen and oxygen species is considered. At temperatures below 6000 K, apart from the inert gaseous species, diatomic nitrogen is present in appreciable concentrations. As this temperature is exceeded, monatomic nitrogen and oxygen concentrations increase significantly. In the Ar–N_2–O_2 plasmas, singly charged argon ions dominate above 14 000 K, whereas in the He–O_2–N_2 plasma, helium atoms dominate up to 17 000 K, above which the concentration of He^+ increases significantly and almost equals the concentration of He at about 22 000 K.

Results of calculations taking into account the formation of NO and its dissociation and ionisation in Ar–8N_2–2O_2 and He–8N_2–2O_2 are shown in Fig. 8*a* and *b*. The NO species distribution in both cases closely follows that of the N_2 species over the entire temperature range considered, and the ionisation of NO is so insignificant that the NO^+ species densities do not fall within the range of the plots. With the exception of the oxygen species, the species present in the plasma phase display much the same trends as for cases assuming no interaction. In contrast, there are significant changes in the number densities for both O_2 and O at temperatures below 6000 K. As the temperature is increased above 6000 K, however, the species density distributions for both O_2 and O become the same as those for the calculations assuming no interaction, i.e. ignoring the formation of species containing both nitrogen and oxygen. This temperature approximately matches the temperature for complete dissociation of NO, as shown in Fig. 2.

Enhancement of the nitrogen concentration in the weld metal with the addition of oxygen bearing gases to the arc is well documented in the literature.[2,25,37,38] Detailed calculations of the species densities, considering the interaction between nitrogen and oxygen, can provide a definitive scientific basis for this behaviour. These calculations show that the formation of NO increases the number density of monatomic nitrogen species in the plasma. Figure 9 shows that the monatomic nitrogen number density in Ar–8N_2–2O_2 plasmas exceeds the monatomic nitrogen number density of an Ar–8N_2 plasma at temperatures less than approximately 8000 K. One measure of this increase is in the effect of oxygen additions on the temperature for complete dissociation of the diatomic species and the point at which monatomic nitrogen dominates over other nitrogen bearing species in the plasma. For example, with oxygen present, the monatomic nitrogen number density exceeds that of diatomic nitrogen at a temperature of less than 6000 K, compared with 7000 K with no oxygen. This decrease in the temperature for complete dissociation accentuates the importance of the dissociation of NO in increasing the number density of monatomic nitrogen in the plasma phase at lower temperatures. A higher number density of monatomic nitrogen with the addition of oxygen to the plasma phase is therefore responsible for the higher nitrogen concentrations observed in the weld metal.

Knowledge of the electron density is necessary to calculate plasma transport properties, especially the electrical conductivity, important in the analysis of the welding arc. Dunn and Eagar[42] investigated the role of metal vapour additions to the GTA welding arc on the electrical and thermal conductivities. They found that small additions of these metals have no significant effect on the transport properties of the arc. In the present work, the effects of diatomic gas additions on the electron density of pure inert gaseous plasmas have been examined.

Figure 10*a–c* shows the calculated electron densities for pure gases, for argon–diatomic gas mixtures, and for helium–diatomic gas mixtures, respectively. The calculated results in Fig. 10*a* show that pure argon, nitrogen, and oxygen are roughly equivalent in their capacity to donate electrons to the plasma phase over the entire temperature range investigated. This effect is further illustrated in Fig. 10*b*, where it is shown that additions of nitrogen and oxygen to argon plasmas have little effect on the overall electron density for the argon based gas mixtures. However, there are fairly sizable differences between the electron densities of argon and helium gases over the same temperature range in Fig. 10*a*, given the much higher ionisation energy for helium. In the helium–diatomic gas mixtures, as shown in Fig. 10*c*, the additions of oxygen and nitrogen increase the overall electron density above that for the pure helium gas.

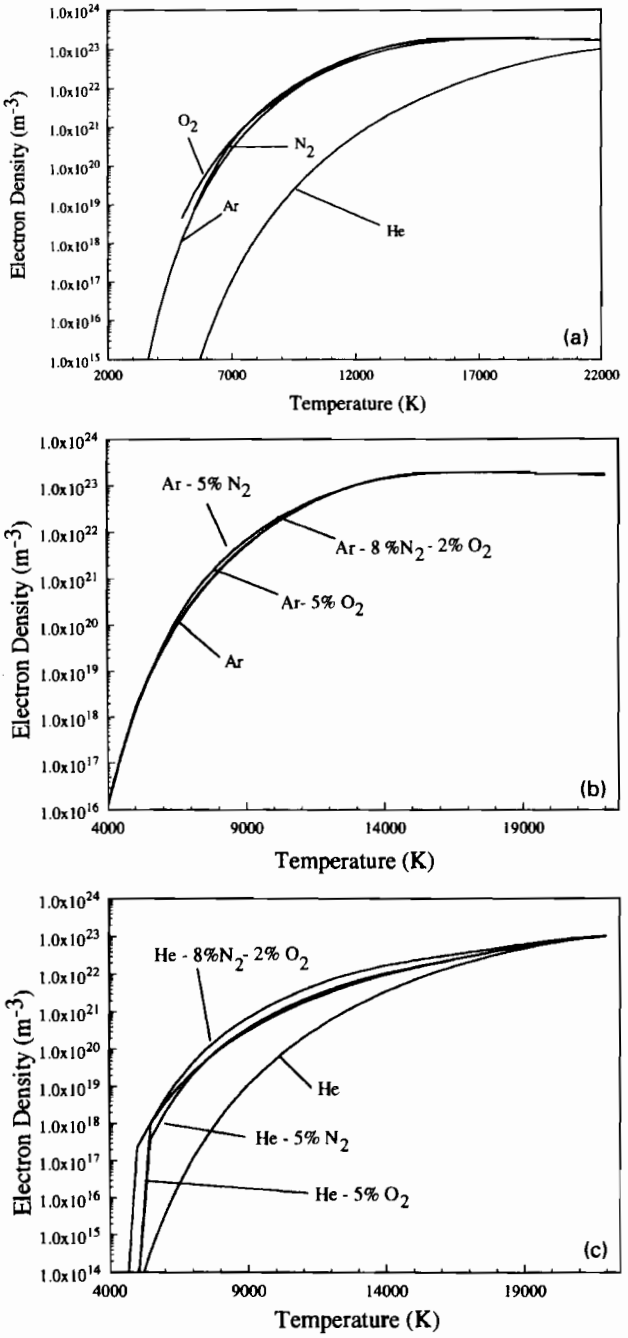

10 Comparison of computed total electron densities for *a* pure gases, *b* argon–diatomic gas mixtures, and *c* helium–diatomic gas mixtures

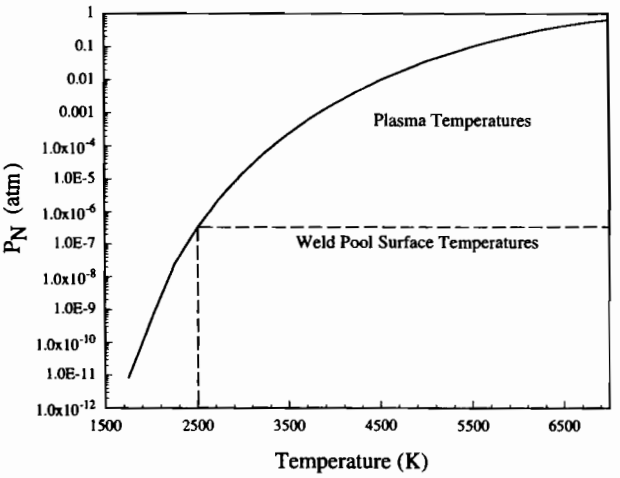

11 Comparison between computed monatomic nitrogen partial pressures in temperature range characteristic of temperature gradient across anode fall region and monatomic nitrogen partial pressure at weld pool surface temperature of 2500 K

It is straightforward to convert the number densities determined above to partial pressures for each species of interest. Figure 11 shows that the partial pressure of monatomic nitrogen in the plasma is significantly higher than that at equilibrium with diatomic nitrogen at the temperatures prevailing at the workpiece surface. For example, at a surface temperature of 2250 K, the atomic nitrogen partial pressure in equilibrium with diatomic nitrogen is $2{\cdot}42 \times 10^{-8}$ atm, whereas the atomic nitrogen partial pressure in a nitrogen plasma at 2500 K is $3{\cdot}17 \times 10^{-7}$ atm. Over the temperature range shown in Fig. 11, which is indicative of the temperatures close to the weld pool surface, the monatomic nitrogen partial pressure can vary by up to six orders of magnitude over a small distance.

Once the monatomic nitrogen partial pressure above the weld metal is determined, the resulting equilibrium nitrogen concentration in the weld metal can then be calculated. Figure 12*a* shows the computed equilibrium nitrogen concentration in pure iron as a function of arc and sample temperatures for an Ar–1N_2 gas mixture. In this figure, the nitrogen dissociation reaction is controlled by the arc temperature, whereas the nitrogen absorption reaction is controlled by the sample temperature. Even at this low level of nitrogen gas input, the monatomic nitrogen partial pressure is sufficient to cause nitrogen saturation in the sample at relatively low arc temperatures. For example, as shown in Fig. 12*a* and *b*, the nitrogen solubility increases rapidly with increasing arc temperature until at an arc temperature of 5000 K, liquid iron is saturated with nitrogen at all sample temperatures. This level of nitrogen saturation is controlled by the solubility of diatomic nitrogen in iron at 1 atm pressure at the temperature on the weld pool surface.[34] Nitrogen saturation in the weld metal can lead to the formation of gas bubbles and pinholes during the solidification of weld metals and arc melted iron, thus degrading the properties of the weld.[34] It can also be inferred that arc temperatures at levels approaching 100–200 K above the sample temperature provide sufficient monatomic nitrogen to the metal surface to increase the nitrogen concentration significantly, this being very similar to the assumptions found in previous models.

A higher solubility of monatomic nitrogen in iron is observed at lower temperatures, as predicted by equilibrium calculations, and the nitrogen saturation limit is reached at fairly low arc temperatures. For example, at 1850 K an iron sample theoretically reaches the nitrogen saturation limit at an arc temperature approximately 100 K lower than for a sample at 2400 K. The sample temperature and nitrogen solubility are compared for various arc temperatures in Fig. 12*c*, in which the range of sample temperatures at which nitrogen saturation is reached rapidly increases as the arc temperature is increased. At these temperatures, the diatomic nitrogen species is significantly dissociated into the monatomic species and the partial pressure of monatomic nitrogen reaches exceptionally high levels, of the order of approximately 0·001 atm for an Ar–1N_2 gas mixture.

EMISSION SPECTROSCOPY OF GLOW DISCHARGES

The suitability of glow discharges to model several important features of welding plasmas has been previously addressed,[31,35] and an experimental apparatus used in these

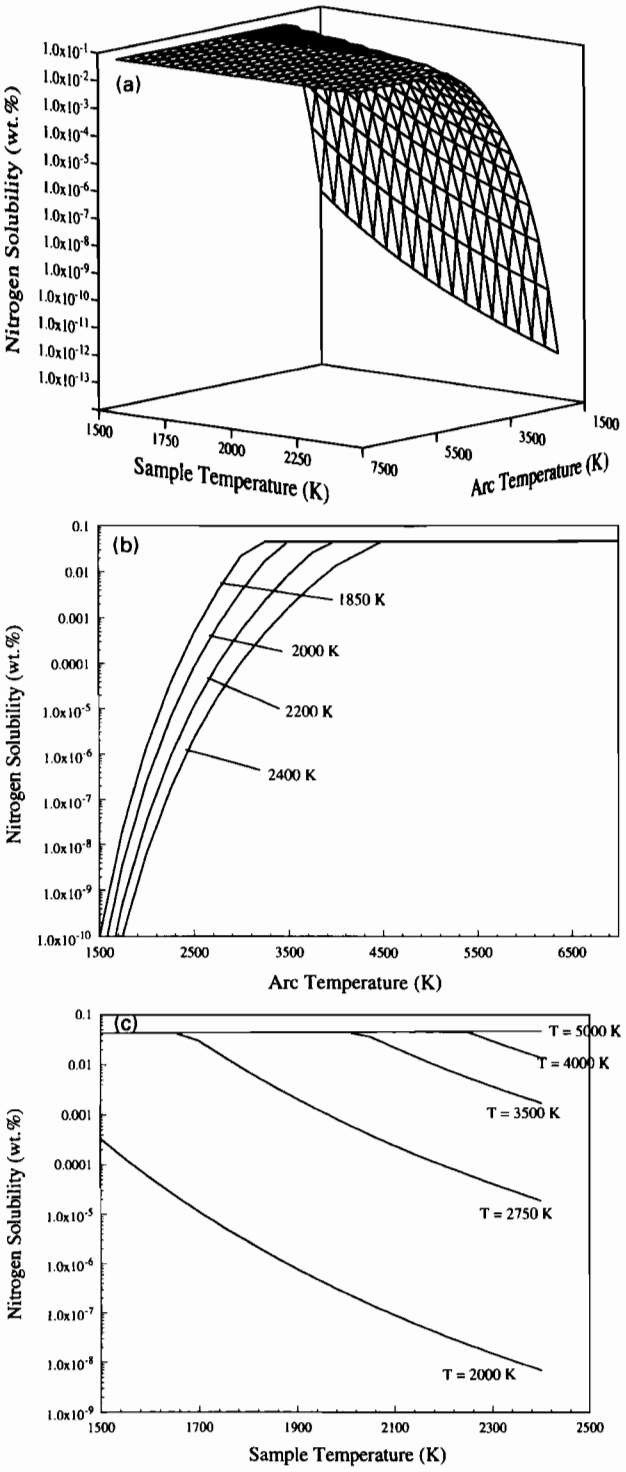

12 Nitrogen solubility in pure iron in contact with Ar–1N_2 plasma *a* determined as function of arc temperature and sample temperature, characteristic of weld pool surface, *b* plotted as function of arc temperature for several sample temperatures, and *c* plotted as function of sample temperature for several arc temperatures

previous studies and described in the literature[35] has been utilised here to analyse glow discharges composed of nitrogen and oxygen mixtures. A systematic analysis of glow discharge plasmas using emission spectroscopy techniques can validate the existence of species present in the plasma phase. Plasmas with the same compositions as those for which calculations were performed have been analysed to determine the species present using standard references.[53,54]

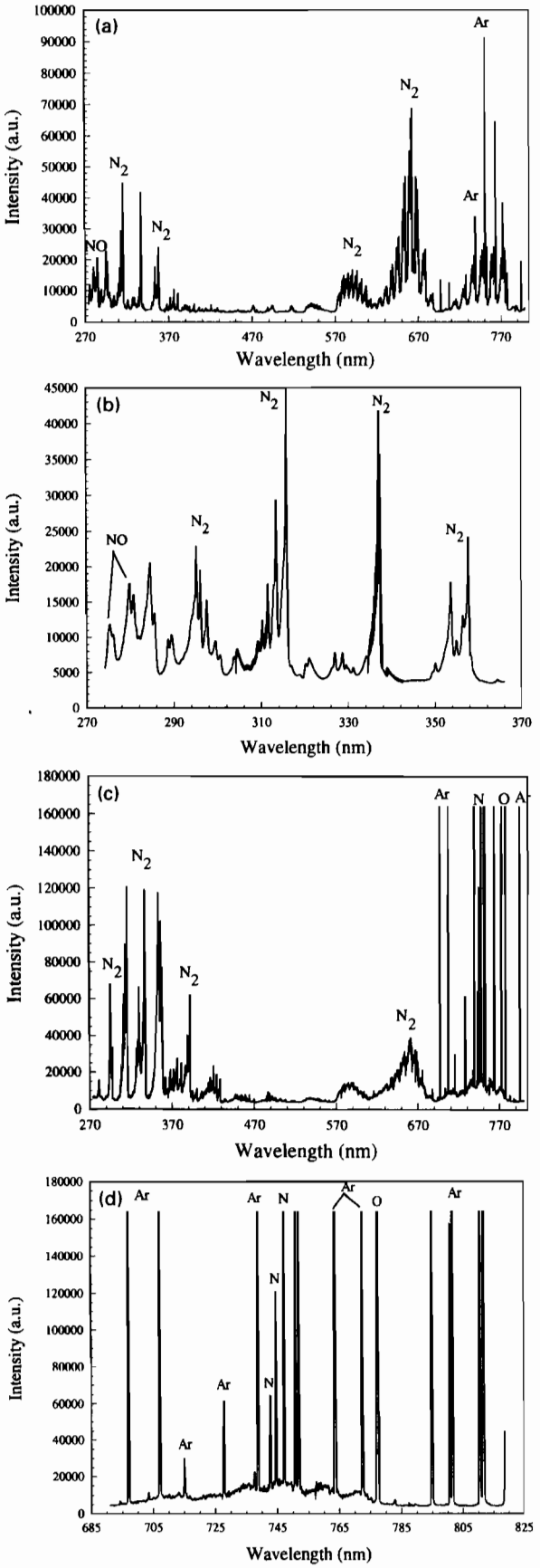

13 *a* emission spectrum for low temperature Ar–8N_2–2O_2 glow discharge plasma, *b* portion of same spectrum with NO peaks highlighted, *c* emission spectrum for high temperature Ar–8N_2–2O_2 glow discharge plasma, and *d* portion of same spectrum with N and O peaks highlighted

Table 3 Summary of important constants

Constant	Definition	Value
m_e	Rest mass of electron	$9{\cdot}11 \times 10^{-31}$ kg
k	Boltzmann's constant	$1{\cdot}38 \times 10^{-23}$ J K^{-1}
		$8{\cdot}62 \times 10^{-5}$ eV K^{-1}
		0·695 cm^{-1}
h	Planck's constant	$6{\cdot}63 \times 10^{-34}$ J s
		$4{\cdot}14 \times 10^{-15}$ eV s
c	Speed of light	$3{\cdot}0 \times 10^{10}$ cm s^{-1}

Glow discharges with both low and high electron temperatures have been analysed. At low electron temperatures, below approximately 5000 K, there is a significant molecular nitrogen component to the spectra analysed. In addition, NO peaks are present in the spectra, indicating a reaction between the nitrogen and oxygen in the plasma phase. A representative spectrum for a low temperature glow discharge, of the order of approximately 5000 K, for an $Ar–8N_2–2O_2$ gas mixture is shown in Fig. 13*a*, with the NO peaks highlighted in Fig. 13*b*. As the electron temperature of the plasma is increased to levels greater than 7000 K, shown in Fig. 13*c* and *d* for an $Ar–8N_2–2O_2$ gas mixture, the NO peaks disappear and peaks for the monatomic species, i.e. N and O, become more dominant, even showing traces of ionic components. Figure 13*c* shows a representative spectrum for a higher temperature glow discharge, with the peaks for the monatomic nitrogen species highlighted in Fig. 13*d*. Thus, the use of emission spectroscopy provides definitive proof for the presence of NO at low electron temperatures and validates the conclusions from the comprehensive calculations performed here.

Table 4 Summary of electronic energy levels for various species: from Ref. 56

Energy level designation	J	Energy, cm^{-1}	g
Nitrogen atoms (N)			
$2p^3\ ^4S^0$	$1\frac{1}{2}$	0	4
$2p^3\ ^2D^0$	$2\frac{1}{2}$	19 224·464	6
	$1\frac{1}{2}$	19 233·177	4
$2p^3\ ^2P^0$	$1\frac{1}{2}$	28 838·92	2
	$\frac{1}{2}$	28 839·306	4
Nitrogen atomic ions (N^+)			
$2p^2\ ^3P$	0	0	1
	1	48·7	3
	2	130·8	5
$2p^2\ ^1D$	2	15 316·2	5
$2p^2\ ^1S$	0	32 688·8	1
$2p^3\ ^5S^0$	2	46 784·6	5
Oxygen atoms (O)			
$2p^4\ ^3P$	2	0	5
	1	158·265	3
	0	226·977	1
$2p^4\ ^1D$	2	15 867·862	5
$2p^4\ ^1S$	0	33 792·583	1
Oxygen atomic ions (O^+)			
$2p^3\ ^4S^0$	$1\frac{1}{2}$	0	4
$2p^3\ ^2D^0$	$2\frac{1}{2}$	26 808	6
	$1\frac{1}{2}$	26 830·5	4
$2p^3\ ^2P^0$	$1\frac{1}{2}$	40 466·9	4
	$\frac{1}{2}$	40 468·4	2
Oxygen atomic ions (O^{++})			
$2p^2\ ^3P$	0	0	1
	1	113·4	3
	2	306·8	5
$2p^2\ ^1D$	2	20 271	5
$2p^2\ ^1S$	0	43 183·5	1

J spin; g degeneration.

CONCLUSIONS

The nature and concentration of various nitrogen bearing species in the welding arc during GTA welding operations have been determined based on detailed calculations of the partition functions for each nitrogen bearing species. Number density calculations show that neutral monatomic and diatomic species dominate near the surface of the weld pool in GTA welding arcs. Conversely, ionic and atomic species dominate away from the weld pool surface.

The monatomic nitrogen partial pressures in the plasma formed at temperatures higher than those at the weld pool surface cause dramatic increases in the amount of nitrogen absorbed in the weld metal. At plasma temperatures higher than 5000 K, the iron weld pool surface reaches nitrogen saturation at all temperatures. Therefore, the temperature difference between the plasma and the weld metal surface plays a significant role in the enhanced nitrogen dissolution process.

Additions of oxygen into a nitrogen containing plasma, such as the addition of air into the welding arc, affect the species density distributions of both oxygen and nitrogen containing species in the welding arc. Calculations show a significant increase in the number density of monatomic nitrogen gas when oxygen is added to the shielding gas in the welding arc. These calculations therefore provide a conclusive scientific basis to explain the experimentally observed enhancement of nitrogen concentrations with the addition of oxygen to the arc.

There are significant differences in the electron density between an argon and a helium plasma for electron temperatures below approximately 15 000 K. This difference in electron density decreases progressively as the electron temperature increases. Additions of oxygen and nitrogen to pure argon have little effect on the electron density over the range of temperatures investigated. However, when oxygen and nitrogen are added to pure helium, significant increases in the electron density are observed at temperatures below approximately 15 000 K.

Emission spectroscopic studies of glow discharge plasmas containing the same gas compositions as those in the above calculations have also been performed. These studies provide evidence for the existence of NO species in the plasma phase at low temperatures and for the important role of dissociation of diatomic species as the temperature is increased. As a whole, these emission spectroscopic studies reinforce the calculated trends in species densities.

APPENDIX 1

Calculation of partition functions

The partition function of a given species is the product of the partition functions associated with each independent energy mode. In a monatomic gas, the partition function

Table 5 Summary of spectroscopically determined values used in calculation of partition functions for nitrogen molecule N_2 for various energy states: from Ref. 57

Parameter, cm^{-1}	$X(^1\Sigma_g^+)$	$A(^3\Sigma_u^+)$	$B(^3\Pi_g)$	$a(^1\Pi_u)$
A_0	0	49 774	59 328	68 957
ω_e	2359·61	1460·4	1732·84	1692·3
$x_e\omega_e$	14·445	13·93	14·44	13·32
B_e	2·007	1·440	1·643	1·642
α	0·018	0·013	0·018	0·021
D	$5{\cdot}77 \times 10^{-6}$	...	...	...

Table 6 Summary of spectroscopically determined values used in calculation of partition functions for nitrogen molecular ion N_2^+ for various energy states: from Ref. 57

Parameter, cm^{-1}	$X(^2\Sigma_g^+)$	$A(^2\Pi_{ui})$	$B(^2\Sigma_u^+)$	$a(^4\Sigma_u^+)$	$D(^2\Pi_{gi})$
A_0	0	9166·9	25 461·4	25 467	52 318·2
ω_e	2207	1903·7	2419·84	2398	907·7
$x_e\omega_e$	16·10	15·02	23·18	14	11·91
B_e	1·93176	1·7444	2·04756	2·071	1·113
α	0·01881	0·0188	0·024	0·014	0·02
D	$6·10 \times 10^{-6}$	$5·6 \times 10^{-6}$	$6·17 \times 10^{-6}$	...	5×10^{-6}

for each monatomic species Z_i can be defined as follows

$$Z_i = \sum g \exp(-E_i/kT) \quad . . . . . (33)$$

where k is the Boltzmann constant, T is the absolute temperature, and g is the degree of degeneration or statistical weight of the energy level E_i.

The degree of degeneration of an atom is defined as the number of different solutions for independent wave functions which correspond to a given energy level. The degree of degeneration in an atom is expressed in quantum mechanical terms as the value $2l+1$, where l is the quantum number representing the angular momentum component of that energy level.[55] Values for the various constants unique to the atomic species to be analysed are available in standard reference sources.[56] Table 3 shows the values and units required for each of these constants in the solution of this equation and other important equations to follow. In addition, Table 4 shows the constants for the atomic energy levels used in the calculation of the partition functions for the respective atomic and ionic species for nitrogen and oxygen.

The calculation of the partition function for a molecule is much more complex than that for an atom because of its more complex structure with a greater number of energy levels. These various energy levels interact in ways not observed for an atom. In general, the internal modes of energy storage in a molecule are electronic, vibrational, and rotational. The degree of degeneration for a given energy level in a molecule is also affected by this large number of energy levels and the interaction between them. Therefore, the degree of degeneration for a molecule is defined in terms of specific energy levels. Molecular states designated $^n\Sigma$ have degeneracy $g_e = n$ and all other molecular states ($^n\pi$, $^n\Delta$, $^n\Phi$, etc.) have degeneracy $g_e = 2n$ (Refs. 43 and 44).

The internal partition function for molecular species Z_i is the product of the partition functions relating to the different energy modes characteristic of the molecule and is defined by the following relationship

$$Z_i = Z_{el} Z_v Z_r Z_c \quad . . . . . (34)$$

where Z_{el} is the electronic partition function, Z_v is the vibrational partition function, which refers to a harmonic oscillation of the molecule with a frequency corresponding to the distance between the two lowest vibrational levels $\omega_e - 2x_e\omega_e$, Z_r is the rotational partition function, which refers to a rigid rotator with a moment of inertia corresponding to that of the zero point vibration, and Z_c is a correction factor taking into account anharmonicity, centrifugal forces, and interaction between vibration and rotation. The spectroscopically determined constants for each molecular species are available in standard reference books on molecular spectra. These constants are presented[57] in Tables 5–8 for nitrogen and oxygen species.

The electronic partition function for the molecular species Z_{el} is defined in the following relationship

$$Z_{el} = g \exp\left(-A_0 \frac{hc}{kT}\right) \quad . . . . . (35)$$

where g is the degeneracy, A_0 is the energy level in cm^{-1}, h is Planck's constant, c is the speed of light, and T is the electron temperature.

The vibrational partition function for the molecular species Z_v is defined by the relationship

$$Z_v = [1 - \exp(-u)]^{-1} \quad . . . . . (36)$$

where the variable u is defined as follows

$$u = \frac{hc(\omega_e - 2x_e\omega_e)}{kT} \quad . . . . . (37)$$

The rotational partition function Z_r is defined by the relationship

$$\ln Z_r = -\ln 2\sigma + \frac{\sigma}{3} \quad . . . . . (38)$$

where the variable σ is defined by the following relationship

$$\sigma = \frac{hc(B_e - \alpha/2)}{kT} \quad . . . . . (39)$$

where B_e and α are constants which account for the interaction between vibration and rotation. The final correctional partition function Z_c accounts for the interaction between various components of the molecular energy levels and is defined in the following relationship

$$\ln Z_c = \frac{1}{u}(2\gamma + 6\gamma^{1/2}x^{1/2} + 2x) + (3\gamma - 3\gamma^{1/2}x^{1/2} - 2x) + \frac{u}{6}(-3\gamma + 3\gamma^{1/2}x^{1/2} + 5x) - \frac{u^2}{6}x + \frac{u^3}{120}(\gamma - \gamma^{1/2}x^{1/2}) + x \quad . . . . . (40)$$

Table 7 Summary of spectroscopically determined values used in calculation of partition functions for oxygen molecule O_2 for various energy states: from Ref. 57

Parameter, cm^{-1}	$X(^3\Sigma_g^-)$	$a(^1\Delta_g)$	$b(^1\Sigma_g^+)$	$c(^1\Sigma_u^-)$	$A'(^3\Delta_u)$
A_0	0	7918·1	13 195·1	33 057·3	34 690
ω_e	1580·19	1483·5	1432·77	794·29	850
$x_e\omega_e$	11·38	12·9	14·0	12·736	20
B_e	1·44563	1·4246	1·40037	0·915	0·96
α	0·0159	0·0171	0·0182	0·0139	0·026
D	$4·84 \times 10^{-6}$	$4·86 \times 10^{-6}$	$5·35 \times 10^{-6}$	$7·40 \times 10^{-6}$	$5·55 \times 10^{-6}$

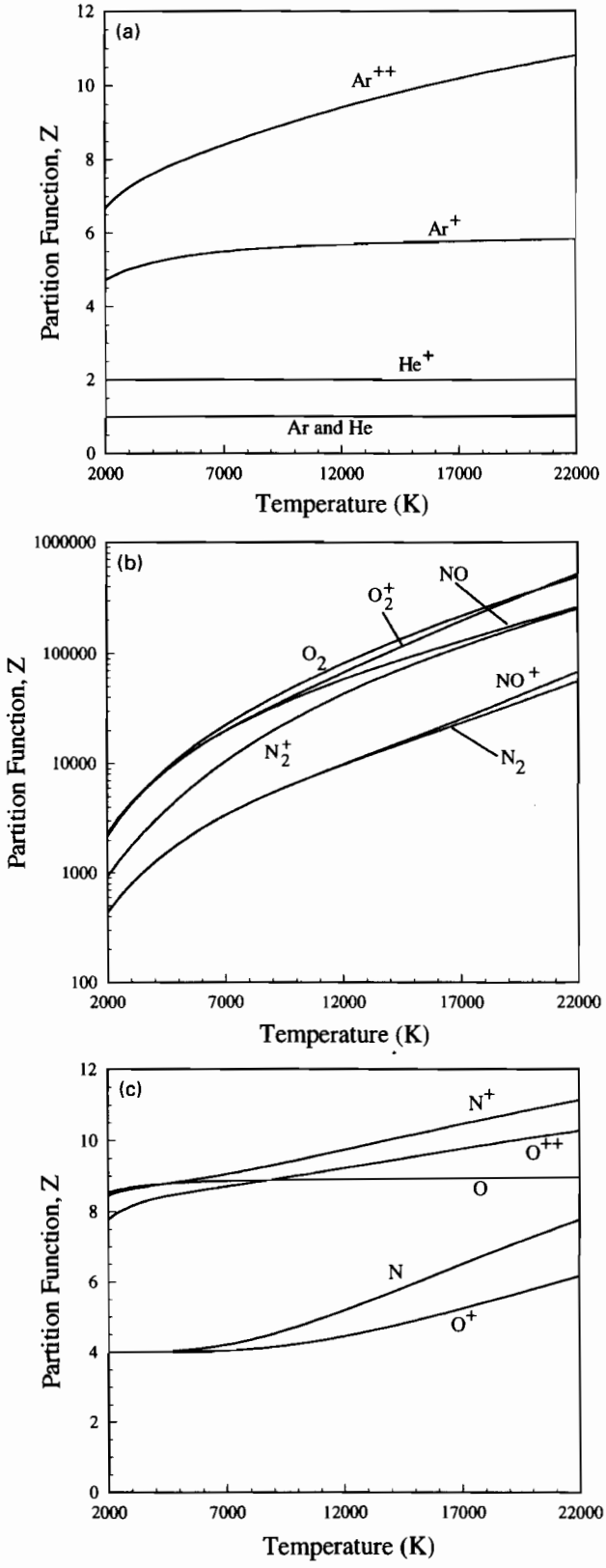

14 Computed partition functions as function of temperature for *a* argon and helium species, *b* molecular oxygen and nitrogen species, and *c* atomic oxygen and nitrogen species in plasma phase

where γ and x are defined in equations (41) and (42)

$$\gamma = \frac{B_e}{\omega_e} \quad \ldots \quad (41)$$

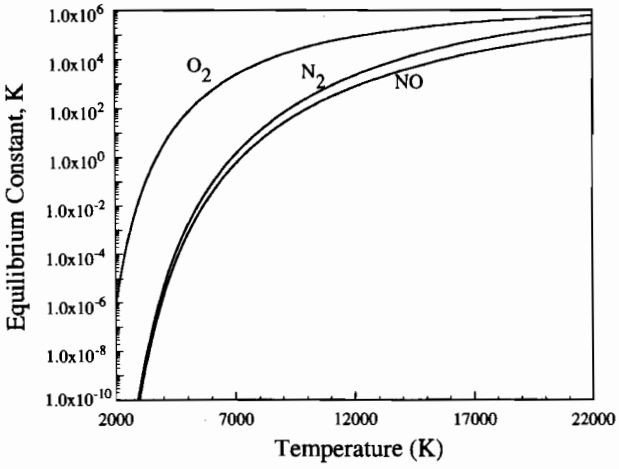

15 Comparison of computed equilibrium constants for dissociation of N_2, O_2, and NO expressed by equations (5), (12), and (26) plotted as function of temperature

$$x = \frac{x_e \omega_e}{\omega_e} \quad \ldots \quad (42)$$

The calculation of internal partition functions Z_i for both atomic and molecular species is necessary for the solution of the Saha–Eggert relation for the ionisation reactions and for the solution of the equilibrium constants for the dissociation reactions of nitrogen and oxygen. For example, partition function calculations are necessary in equations (3), (4), (9)–(11), (15), (16), (19), and (29). Figure 14 shows the calculated partition functions for inert gases and diatomic and monatomic nitrogen and oxygen species as a function of temperature.

APPENDIX 2
Thermodynamic basis for dissociation reaction calculations

The degree of dissociation of a diatomic gas can be computed with knowledge of the free energy of both the molecular and atomic species. These values are calculated from available spectroscopically determined data, which appear in the form of the partition functions. The Helmholtz free energy of one mole of an ideal gas is shown in the following relationship[36]

$$f - u_0 = -kT \ln \left[\frac{ev}{N_A h^3} (2\pi m k T)^{3/2} Z_i \right]^{N_A} \quad \ldots \quad (43)$$

where f is the Helmholtz free energy of one mole of an ideal gas, u_0 is the free energy at absolute zero, e is the base of natural logarithms (2·71828), v is the volume containing the gas, m is the mass of a single molecule, and Z_i is the internal partition function of the species being analysed.

The molar free enthalpy $g - u_0$ can thus be rewritten in the following forms[36]

$$g - u_0 = f - u_0 + pv = f - u_0 + RT \quad \ldots \quad (44)$$

$$-\frac{g - u_0}{T} = \frac{5}{2} R \ln T + \frac{3}{2} R \ln M - R \ln p + R \ln \frac{2^{3/2} \pi^{3/2} e k^{5/2}}{h^3 N_A^{3/2}} - R + R \ln Z_i \quad (45)$$

where $R = kN_A$ is the gas constant, M is the molecular weight, and p is the pressure. Using the relation in equation (45), the molar free enthalpy for each species, i.e. the atomic and molecular nitrogen and oxygen, can be calculated and substituted in the following equations to determine the equilibrium constant.

Table 8 Summary of spectroscopically determined values used in calculation of partition functions for oxygen molecular ion O_2^+ for various energy states: from Ref. 57

Parameter, cm^{-1}	$X(^2\Pi_g)$	$a(^4\Pi_{ui})$	$A(^2\Pi_u)$	$b(^4\Sigma_g^-)$
A_0	0	32 964	40 669·3	49 552
ω_e	1904·77	1035·69	898·25	1196·7
$x_e\omega_e$	16·25	10·39	13·57	17·09
B_e	1·6913	1·1046	1·0617	1·28729
α	0·01976	0·01575	0·01936	0·02206
D	$5·32 \times 10^{-6}$	$4·88 \times 10^{-6}$	$5·94 \times 10^{-6}$	$5·81 \times 10^{-6}$

Since the dissociation reaction defines the conversion of one mole of ideal gaseous N_2 at a pressure of 1 atm to two moles of ideal gaseous N at the same pressure, the Gibbs free energy ΔG° can be defined as follows[36]

$$\Delta G^\circ = 2g^\circ(N) - g^\circ(N_2) \quad . \quad . \quad . \quad . \quad . \quad . \quad . \quad . \quad . \quad . \quad . \quad (46)$$

where g° represents the molar free energies of the ideal gases at the standard pressure. By substituting the relationships for the Gibbs free energy shown above into the definition of the reaction constant and taking into account the statistical mechanical definitions for the dissociation reaction, the following general relation for the equilibrium constant K can be defined[36]

$$\log K = \frac{g^\circ(N_2) - u_0^\circ(N_2)}{RT} - 2\frac{g^\circ(N) - u_0^\circ(N)}{RT} - \frac{\Delta U_0^\circ}{RT} \quad . \quad . \quad . \quad . \quad . \quad . \quad . \quad . \quad . \quad . \quad (47)$$

where ΔU_0° is the dissociation energy at absolute zero deduced from spectroscopic data. Values for each free energy term in equation (47), $g^\circ(i) - u_0^\circ(i)$, are determined in equation (45), and the dissociation energy ΔU_0° for nitrogen, oxygen, and other diatomic molecules is an available constant. For example, nitrogen has a dissociation energy of 9·764 eV, and Table 9 summarises both the ionisation and dissociation energies for both nitrogen and oxygen and other species of interest. Figure 15 also shows the calculated equilibrium constants for the dissociation of N_2, O_2, and NO as a function of temperature. Once the equilibrium constant is determined, it can be substituted into equations (6) for nitrogen, (12) for oxygen, and (27) for NO, and relations for the dissociation reactions thus developed.

ACKNOWLEDGEMENTS

This work was supported by the United States Department of Energy, Office of Basic Energy Sciences, Division of Materials Science, under grant no. DEFG02-84ER45158. One of the authors (TAP) would also like to acknowledge the financial support provided by the AWS Foundation and the Navy Joining Center in the form of an AWS Graduate Research Fellowship.

Table 9 Summary of ionisation and dissociation energies for various gases of interest: all energies listed are relative to ground state of species

Species in arc	Dissociation energy, eV	Ionisation energy, eV
Ar(g)	...	15·755
He(g)	...	24·580
N_2(g)	9·759	15·581
N	...	14·54
O_2(g)	5·115	12·071
O	...	13·614
O^+	...	35·146
NO(g)	6·496	9·264

REFERENCES

1. P. D. BLAKE: *Weld. Res. Int.*, 1979, **9**, (1), 23–56.
2. T. KOBAYASHI, T. KUWANA, and Y. KIKUCHI: *Weld. World*, 1967, **5**, (2), 58–73.
3. T. KUWANA and H. KOKAWA: *Trans. Jpn Weld. Soc.*, 1986, **17**, (1), 20–26.
4. T. KUWANA and H. KOKAWA: *Trans. Jpn Weld. Soc.*, 1988, **19**, (2), 92–99.
5. T. KUWANA, H. KOKAWA, and N. MURAMATSU: *Trans. Jpn Weld. Soc.*, 1989, **20**, (1), 10–16.
6. T. KUWANA, H. KOKAWA, and K. NAITOH: *Trans. Jpn Weld. Soc.*, 1990, **21**, (2), 157–163.
7. T. KUWANA, H. KOKAWA, and S. MATSUZAKI: *Trans. Jpn Weld. Soc.*, 1987, **18**, (1), 12–18.
8. T. KUWANA, H. KOKAWA, and K. NAITOH: *Trans. Jpn Weld. Soc.*, 1986, **17**, (2), 117–123.
9. S. OHNO and M. UDA: *Trans. Natl Res. Inst. Met. (Jpn)*, 1981, **23**, (4), 243–248.
10. M. UDA and S. OHNO: *Trans. Natl Res. Inst. Met. (Jpn)*, 1978, **20**, (6), 358–365.
11. M. UDA and S. OHNO: *Trans. Natl Res. Inst. Met. (Jpn)*, 1973, **15**, (1), 20–28.
12. M. UDA and T. WADA: *Trans. Natl Res. Inst. Met. (Jpn)*, 1968, **10**, (2), 21–33.
13. M. UDA and S. OHNO: *Trans. Natl Res. Inst. Met. (Jpn)*, 1975, **17**, (2), 69–76.
14. M. UDA: *Trans. Natl Res. Inst. Met. (Jpn)*, 1982, **24**, (4), 218–225.
15. G. den OUDEN: *Philips Weld. Rep.*, 1977, **13**, (1), 1–6.
16. G. den OUDEN and O. GRIEBLING: in 'International trends in welding science and technology', (ed. S. A. David and J. M. Vitek), 431–435; 1990, Materials Park, OH, ASM International.
17. J. W. HOOJIMANS and G. den OUDEN: *Weld. J. Res. (Suppl.)*, 1992, **71**, (10), 377s–380s.
18. J. W. HOOJIMANS and G. den OUDEN: *Mater. Sci. Technol.*, 1996, **12**, (1), 81–85.
19. J. W. HOOJIMANS and G. den OUDEN: *Weld. J. Res. (Suppl.)*, 1997, **76**, (7), 264s–268s.
20. S. HERTZMAN, R. J. PETTERSSON, R. BLOM, E. KIVINEVA, and J. ERIKSSON: *ISIJ Int.*, 1996, **36**, (7), 968–976.
21. J. M. ROBINSON, R. C. REED, and A. CAMYAB: in 'Trends in welding research', (ed. H. B. Smartt *et al.*), 499–504; 1996, Materials Park, OH, ASM International.
22. C. E. CROSS, H. HOFFMEISTER, and G. HUISMANN: Proc. IIW Annual Assembly, Stockholm, Sweden, June 1995, IIW.
23. T. A. PALMER, K. MUNDRA, and T. DEBROY: in 'Mathematical modelling of weld phenomena 3', (ed. H. Cerjak), 3–40; 1997, London, The Institute of Materials.
24. T. KUWANA, H. KOKAWA, and M. SAOTOME: in 'Mathematical modelling of weld phenomena 3', (ed. H. Cerjak), 64–81; 1997, London, The Institute of Materials.
25. C. J. ALLUM: *Weld. Res. Counc. Bull.*, 1991, **369**, 68–84.
26. R. MENON and D. J. KOTECKI: *Weld. Res. Counc. Bull.*, 1991, **369**, 141–161.
27. T. KUWANA: in 'Advanced joining technologies', (ed. T. H. North), 117–128; 1990, New York, Chapman and Hall.
28. J. D. KATZ and T. B. KING: *Metall. Trans.*, 1989, **20B**, 175–185.
29. T. EL GAMMAL, B. YOSTOS, and F. N. EL SABBAHY: *Steel Res.*, 1992, **63**, (6), 234–241.
30. T. EL GAMMAL, R. ABDEL-KARIM, M. T. WALTER, E. WOSCH, and S. FELDHAUS: *ISIJ Int.*, 1996, **36**, (7), 915–921.
31. A. BANDOPADHYAY, A. BANERJEE, and T. DEBROY: *Metall. Trans.*, 1992, **23B**, 207–214.

32. V. I. LAKOMSKII and G. F. TORKHOV: *Sov. Phys. Dokl.*, 1969, **13**, (11), 1159–1161.
33. S. A. GEDEON and T. W. EAGAR: *Weld. J. Res. (Suppl.)*, 1990, **69**, 264s–271s.
34. K. MUNDRA and T. DEBROY: *Metall. Mater. Trans.*, 1995, **26B**, (2), 149–157.
35. T. A. PALMER and T. DEBROY: *Weld. J. Res. (Suppl.)*, 1996, **75**, (7), 197s–207s.
36. J. D. FAST: *Philips Res. Rep.*, 1947, **2**, 382–398.
37. V. I. GALINICH and V. V. PADGAETSKII: *Avtom. Svarka*, 1961, **16**, (2), 24–32.
38. I. K. POKHODNYA and A. P. PAL'TSEVICH: *Avtom. Svarka*, 1971, **25**, (2), 8–11.
39. R. D. PEHLKE and J. F. ELLIOTT: *Trans. AIME*, 1960, **218**, 1088–1101.
40. H. M. J. PFLANZ: PhD thesis, Technical University, Eindhoven, The Netherlands, 1967.
41. G. J. DUNN, C. D. ALLEMAND, and T. W. EAGAR: *Metall. Trans.*, 1986, **17A**, 1851–1863.
42. G. J. DUNN and T. W. EAGAR: *Metall. Trans.*, 1986, **17A**, 1865–1871.
43. K. S. DRELLISHAK, D. P. AESCHLIMAN, and A. B. CAMBEL: *Phys. Fluids*, 1965, **8**, (9), 1590–1600.
44. K. S. DRELLISHAK, C. F. KNOPP, and A. B. CAMBEL: *Phys. Fluids*, 1963, **6**, (9), 1280–1288.
45. J. F. KEY, J. W. CHAN, and M. E. McILWAIN: *Weld. J. Res. (Suppl.)*, 1983, **62**, (7), 179s–184s.
46. A. E. F. GICK, M. B. C. QUIGLEY, and P. H. RICHARDS: *J. Phys. D, Appl. Phys.*, 1973, **6**, 1941–1949.
47. J. WENDELSTORF, I. DECKER, H. WOHLFAHRT, and G. SIMON: in 'Mathematical modelling of weld phenomena 3', (ed. H. Cerjak), 848–897; 1997, London, The Institute of Materials.
48. C. S. WU, M. USHIO, and M. TANAKA: *Comput. Mater. Sci.*, 1997, **7**, 308–314.
49. G. N. HADDAD and A. J. D. FARMER: *Weld. J.*, 1985, **64**, (12), 339s–342s.
50. A. J. D. FARMER, G. N. HADDAD, and L. E. CRAM: *J. Phys. D, Appl. Phys.*, 1986, **19**, 1723–1730.
51. R. T. C. CHOO, J. SZEKELY, and R. C. WESTHOFF: *Metall. Trans.*, 1992, **23B**, 357–369.
52. G. N. HADDAD and A. J. D. FARMER: *J. Phys. D, Appl. Phys.*, 1984, **17**, 1189–1196.
53. R. W. B. PEARSE and A. G. GAYDON: 'The identification of molecular spectra', 4th edn; 1976, New York, Chapman and Hall.
54. G. R. HARRISON *et al.*: 'MIT wavelength tables'; 1982, Cambridge, MA, Massachusetts Institute of Technology Press.
55. J. AVERY: in 'The quantum theory of atoms, molecules, and photons', 77–79; 1972, New York, McGraw-Hill.
56. C. E. MOORE: 'Atomic energy levels', NSRDS-NBS 35, Vol. 1–3; 1971, Washington, DC, National Bureau of Standards.
57. G. HERZBERG: 'Molecular spectra and molecular structure', Vol. 4, 'Constants of diatomic molecules'; 1979, New York, Van Nostrand.